Megakaryocytes assemble a three-dimensional cage of extracellular matrix that controls their maturation and anchoring to the vascular niche

Claire Masson[1≠], Cyril Scandola[2≠], Jean-Yves Rinckel[1], Fabienne Proamer[1], Emily Janus-Bell[1], Fareeha Batool[1], Naël Osmani[3], Jacky G. Goetz[3], Léa Mallo[1], Catherine Léon[1], Alicia Bornert[1], Renaud Poincloux[4], Olivier Destaing[5], Alma Mansson[6], Hong Qian[6], Maxime Lehmann[1], Anita Eckly[1]

≠ First co-authors ship

[1]Université de Strasbourg, INSERM, EFS Grand Est, BPPS UMR_S1255, FMTS, F-67065 Strasbourg, France ; [2]Institut Pasteur, Université Paris Cité, Ultrastructural Bioimaging Unit, 75015 Paris, France ; [3]INSERM UMR_S1109, Tumor Biomechanics Lab, Université de Strasbourg, Fédération de Médecine Translationnelle de Strasbourg (FMTS), Strasbourg, F-67000, France. Equipe Labellisée Ligue Contre le Cancer; [4] Institut de Pharmacologie et de Biologie Structurale, Université de Toulouse, CNRS, UMR5089, 205 route de Narbonne, BP64182 31077 Toulouse, France ; [5] Institute for Advanced Biosciences, Centre de Recherche Université Grenoble Alpes, Inserm U 1209, CNRS UMR 5309, Grenoble, France; [6] Center for Hematology and Regenerative Medicine (HERM), Department of Medicine Hiddinge, Karolinska University Hospital, Karonlinska Institute, Stockholm, Sweden.

Key words : Megakaryocyte, extracellular matrice, intravasation, integrins, proteolysis

Number of figures : 7

Correspondance to: Anita ECKLY
UMR-S1255 INSERM-Université de Strasbourg
Etablissement Français du Sang-Grand Est
10, rue Spielmann, B.P. N°36
67065 Strasbourg Cedex, France
anita.michel@efs.sante.fr
Tel: (33) 388 21 25 25
Fax: (33) 388 21 25 21

Key Points

1. Megakaryocytes form a three-dimensional (3D) cage composed of laminin and collagen IV connected to the basement membrane surrounding them. This microarchitecture stabilizes megakaryocytes within their vascular niche.

2. β1/β3 integrins and MMP are key ECM cage regulators that assist megakaryocyte maturation and intravasation at the bone marrow-blood interface.

Abstract

Megakaryocytes, the progenitor cells of blood platelets, play a crucial role in hemostasis by residing in the bone marrow and ensuring continuous platelet production. Unlike other hematopoietic cells, megakaryocytes do not enter the blood circulation intact. They remain anchored within the bone marrow while extending cytoplasmic protrusions called proplatelets through the sinusoidal endothelial barrier. These proplatelets subsequently fragment into functional platelets. This unique process of intravasation facilitates efficient platelet production while maintaining the megakaryocyte cell body within the bone marrow niche, thus preventing potential thrombotic complications. How the extracellular matrix (ECM) influences the delicate balance between megakaryocyte retention and proplatelet extension remains largely unknown. Here, we investigate the spatial organization and functional role of ECM components in the megakaryocyte vascular niche. Our findings reveal that laminin and collagen IV form three-dimensional (3D) ECM cages encompassing megakaryocytes and anchor them to the sinusoidal basement membrane. Gene deletion shows the existence of laminin α4 in the ECM cage that is necessary to maintain megakaryocyte-sinusoid interactions. Notably, megakaryocytes actively contribute to the ECM cage assembly; β1/β3 integrin knockout weakens these structures, increasing intravasation and entire megakaryocyte entry into circulation. The retention of megakaryocytes by these 3D ECM cages depends on dynamic remodeling processes. Inhibition of ECM proteolysis results in denser cage formation, increasing the frequence of immature megakaryocytes with impaired demarcation membrane system (DMS) development. Thus, the ECM cage represents a novel concept of an active and dynamic 3D microenvironment that is continuously remodeled and essential for maintaining megakaryocyte perivascular positioning. This specific microarchitecture guides megakaryocyte maturation and intravasation, underscoring the critical role of ECM microarchitecture and dynamics in megakaryocyte function.

INTRODUCTION

Megakaryocytes, the precursors of blood platelets, differentiate from hematopoietic stem cells and mature in a complex bone marrow microenvironment. Megakaryocytes are large, highly polyploid cells that contain a complex invaginated network of membranes, known as the demarcation membrane system (DMS), which serves as a membrane reservoir for platelet production. In contrast to other hematopoietic cells, megakaryocytes exhibit a unique platelet production process. They do not enter the bloodstream intact. Instead, they remain anchored in the bone marrow and extend cytoplasmic protrusions called proplatelets through the sinusoidal endothelial barrier. These protrusions protrude into the lumen of bone marrow sinusoids, where they undergo fragmentation to release individual platelets into the circulation. This distinctive mechanism allows for the efficient production and release of platelets while maintaining the megakaryocyte cell body within the bone marrow microenvironment, thus reducing the risk of thrombotic complications (Stone et al., 2022, Boscher et al., 2020). The remaining cell body, composed of a nucleus surrounded by a thin rim of cytoplasm (called the splenocyte), is ultimately phagocytosed in the stroma (Radley and Haller, 1983).

Megakaryocytes are strategically located at the interface between the bone marrow and the blood circulation, specifically at the parasinusoidal region (Lichtman et al., 1978, Stegner et al., 2017). Intravasation, the coordinated passage of megakaryocyte fragments through the sinusoidal barrier, requires an original, complex, and dynamic adaptation of megakaryocytes to highly different microenvironments, both mechanically and biologically. They are positioned next to the endothelial lining and its underlying basement membrane, in equilibrium between the constrained 3D environment of the bone marrow and the fluid environment of the blood. In this context, they are in contact with two types of ECM organization: basement membrane and interstitial ECM.

Megakaryocytes actively influence their structural microenvironment through several ECM remodeling mechanisms, including the endocytosis of plasma proteins like fibrinogen, and the synthesis and release of extracellular matrix (ECM) components such as fibronectin laminin, and type IV collagen (Malara et al., 2014, Abbonante et al., 2017b, Handagama et al., 1987). Additionally, they produce ECM-modifying proteins, including matrix metalloproteinases (MMPs), tissue inhibitors of metalloproteinases (TIMPs), and lysyl oxidase

(LOX), which facilitate the continuous renewal and regulation of the matrix (Malara et al., 2018b, Eliades et al., 2011, Villeneuve et al., 2009). Furthermore, we have recently discovered that megakaryocytes could remodel the substrate-bound fibronectin matrix into basal fibrillar structures surrounding the cells. The extent of fibrillogenesis depended on the stiffness of the substrate, and relied on both β1 and β3 integrins (Guinard et al., 2023). This intricate interplay between megakaryocytes and their surrounding ECM remodeling demonstrates the dynamic nature of the vascular niche and highlights its critical role in platelet production.

The ECM surrounding megakaryocytes plays a crucial role in their development and function. Numerous studies have identified essential components of this matrix, including collagen IV, fibronectin, fibrinogen, and laminin (Larson and Watson, 2006, Malara et al., 2014, Semeniak et al., 2016, Susek et al., 2018). The presence and function of collagen I fibers remain a subject of ongoing debate, with some researchers proposing that they guide megakaryocyte proplatelets toward sinusoids (Oprescu et al., 2022). *In vitro* studies have shown that while collagen I may inhibit proplatelet formation, other ECM components, like collagen IV, fibrinogen, and fibronectin, can facilitate this process (Balduini et al., 2008, Sabri et al., 2004, Malara et al., 2014). The diverse and sometimes contradictory roles of these ECM components in megakaryocyte behavior underscore the complexity of this research area and highlight the need for further investigation, particularly *in vivo*.

The present study provides new insight into the spatial organization of the ECM that envelops megakaryocytes, elucidating its specific architecture and molecular mechanisms governing its dynamics and function. We performed advanced 2D and 3D analyses of mouse bone marrow and identified a novel ECM cage containing laminin chains ϒ1 and α4 and collagen IV that anchored megakaryocytes to the sinusoidal basement membrane. Deleting laminin α4 impairs the connections between megakaryocytes and sinusoids. Megakaryocytes act actively in forming and maintaining this ECM cage, relying on their integrins β1 and β3. Deleting these integrins causes significant impairment of the cage's integrity, resulting in increased intravasation of megakaryocytes and an unexpected release of intact megakaryocytes into the bloodstream. Moreover, *in vivo*, matrix metalloproteinases (MMPs) inhibition reveals that dynamic ECM remodeling is crucial for maintaining the cage structure and supporting megakaryocyte development. In conclusion, our study unveils a 3D ECM cage that physically stabilizes megakaryocytes within their vascular niche. This structure facilitates

the physiological regulation of megakaryocyte maturation and intravasation at the bone marrow-bloodstream interface.

RESULTS

Laminin and collagen IV create a 3D cage around sinusoid-associated megakaryocytes

How the ECM is organized around megakaryocytes within the vascular niche remains to be discovered, as its observation involves technical *in vivo* challenges. We first used ultrathin (250 nm) cryosections and examined ECM composition around megakaryocytes and sinusoids, using GPIbβ and FABP4, respectively (Figure 1A). Our findings revealed that laminin ϒ1 chains and collagen IV delineated the basement membrane underlying the endothelium of sinusoids and the outer contour of mature megakaryocytes (Figure 1A, Suppl. Figure 1Aa). Adjacent cells exhibited granular staining for laminin ϒ1 and collagen IV, which may indicate a potential contribution to the ECM constitution (Suppl. Figure 1Ag-h). Fibronectin was detected in the basement membrane and around megakaryocytes, while fibrinogen was more widespread, associated with the basement membrane, the megakaryocyte surface, and intracellular granules (Suppl. Figure 1Ab-c). Von Willebrand factor (VWF) signal was restricted to the alpha granules of megakaryocytes (Suppl. Figure 1Ad). We observed no detectable signals for type I and III collagen around megakaryocytes or sinusoids despite using two antibodies validated on positive controls (Suppl. Figure 1Ae-f, Suppl. Figure 1B).

Having established the expression of laminin ϒ1, collagen IV, fibronectin, and fibrinogen in the direct megakaryocyte microenvironment, their spatial organization was next investigated using 3D imaging of whole-mount BM preparations (Figure 1B). Analysis of maximum Z-stack projections revealed that laminin ϒ1 and collagen IV formed a reticular 3D ECM cage completely enveloping megakaryocytes and extending radially from the sinusoidal basement membrane (Figure 1B-C). A 3D representation is shown in movie 1. Quantification showed that 92.8 ± 3.3 % of sinusoid-associated megakaryocytes (sMK) have a laminin cage, compared to only 11.4 ± 4.8 % of megakaryocytes in the parenchyma (pMK) (Suppl. Figure 1C). This indicates that the full assembly of the 3D ECM cage required megakaryocyte interaction with the sinusoidal basement membrane. Megakaryocytes in the parenchyma (pMK), which represented a small fraction of the total megakaryocyte population, were characterised by the presence of only a sparse, filigree-like interstitial laminin ϒ1 network in their vicinity (Suppl. Figure 1C). The ECM cage was present at all stages of megakaryocyte maturation, including megakaryocytes with proplatelet extension (Suppl. Figure 1D). Remarkably, freshly isolated bone marrow-derived megakaryocytes maintained their laminin ϒ1 cage after

mechanical dissociation and size exclusion, indicating strong physical attachments between both components (Figure 1D). The 3D arrangement of fibronectin and fibrinogen around megakaryocytes was also analyzed. Although fibronectin and fibrinogen were readily detected around megakaryocytes, a reticular network around megakaryocytes was not observed. Furthermore, no connection was identified between fibronectin and fibrinogen deposition with the sinusoid basement membrane, in contrast to the findings for laminin and collagen IV (Suppl. Figures 1E). These observations demonstrate that megakaryocytes establish precise and tight interactions with an ECM cage made of laminin ϒ1 and collagen IV in a spatially confined microenvironment at the sinusoidal basement membrane.

Reduced 3D laminin cage and vessel-associated megakaryocytes in Lama4$^{-/-}$ mouse bone marrow.

Among the γ1 chain-bearing laminin isoforms, laminin α4 was abundantly found in bone marrow sinusoid basement membrane (Susek et al., 2018). To investigate the direct influence of ECM organization on megakaryocytes, we utilized laminin α4-deficient mice (*Lama*4$^{-/-}$). These mice exhibit mild thrombocytopenia, with platelet counts approximately 20% lower than wild-type (WT) mice (Cai et al., 2023). Using an antibody that targets the laminin γ1 chains, we found a reduced laminin expression around megakaryocytes and in the sinusoid basement membrane of *Lama*4$^{-/-}$ mice, compared to wt mice. Laminin γ1 deposition on megakaryocyte surfaces and basement membrane was significantly reduced by 1.7 and 2.6 folds compared to WT mice, indicating a disruption in the laminin cage (Figure 2A). While collagen IV was associated with the laminin ϒ1 network in WT mice (Suppl. Figure 2A), our analysis revealed no significant alterations in its deposition, whether in the cage or the sinusoidal basement membrane of *Lama*4$^{-/-}$ mice (Figure 2C), indicating that laminin α4 is not required for the collagen IV cage formation. We further analyzed the megakaryocyte localization in the bone marrow of *Lama*4$^{-/-}$ mice. While the total number of megakaryocytes was similar to that in WT mice, a significant reduction of 1.5 fold was evident in the number of megakaryocytes localized near sinusoids of *Lama*4$^{-/-}$ mouse (Figure 2D). These findings underscore the pivotal function of the laminin α4 cage in sustaining optimal megakaryocyte positioning in proximity to sinusoids.

Integrins maintain the structural properties of the ECM cages.

Integrins play a crucial role in ECM remodeling. To elucidate the molecular mechanisms governing the intricate interactions between megakaryocytes and the ECM cage, we investigate the role of integrins. Megakaryocytes express β1 and β3 integrins as main ECM receptors (Yang et al., 2022). Using conformation-independent antibodies, we showed the presence of β1 isoforms on the plasma membrane and DMS (Figure 3A). Similar findings were obtained for total β3 integrins (Suppl. Figure 3A). In contrast, the activated form of β1 integrin was expressed only at interaction sites with laminin γ1 and collagen IV, suggesting that activated β1 integrins mediate megakaryocyte interactions with the ECM cage (Figure 3B). Activated β3 integrin involvement remains to be determined, as no specific signal was detected by testing two different antibodies (JonA-PE, Pac 1).

To test if integrin-mediated signaling plays a role in the structural assembly of the ECM cage, a transgenic mouse model lacking β1 and β3 integrins in the megakaryocyte lineage was used (*Itgb1*$^{-/-}$*/Itgb3*$^{-/-}$) (Figure 3C). *Itgb1*$^{-/-}$*/Itgb3*$^{-/-}$ mice were generated crossing the two single loxP-flanked lines (β1$^{fl/fl}$ and β3$^{fl/fl}$ mice) with *Pf4-Cre* mice (expressing the Cre recombinase under the control of the *Pf4* promoter). Our analysis revealed a 2.6-fold reduction in laminin γ1 deposition on the megakaryocyte surface in *Itgb1*$^{-/-}$*/Itgb3*$^{-/-}$ mice compared to *Pf4-Cre* control mice. Furthermore, intensity profiles demonstrated that laminin γ1 forms a less dense network around the megakaryocytes in the knockout mice, with significantly increased mesh sizes (10.6 ± 1.3 µm vs 6.3 ± 0.6 µm, respectively). Notably, this lower ECM density surrounding megakaryocytes in *Itgb1*$^{-/-}$*/Itgb3*$^{-/-}$ mice is not linked to increased matrix degradation or reduced laminin synthesis (Suppl. Figures 3B and C). As expected, the organization and density of the laminin γ1 network at the basement membrane remained unaffected in these mice, as the integrin deletion is restricted to megakaryocytes (Suppl. Figure 3E).

Further confocal and immunoEM examination revealed a decrease in the expression of fibrillar fibronectin around *Itgb1*$^{-/-}$*/Itgb3*$^{-/-}$ megakaryocytes, along with mislocalization of fibrinogen in the extracellular space of the DMS instead of the granules (Suppl. Figures 3E and 3F). These findings show that megakaryocytes function as architects for their ECM microenvironment (ECM cage and fibronectin, fibrinogen deposition) and that megakaryocytes β1 and β3 integrins are required.

Normal ECM organization is essential for proper megakaryocyte intravasation.

Next, we investigate the relevance of the ECM cage to megakaryocyte functions. We previously described that *Itgb1*$^{-/-}$/*Itgb3*$^{-/-}$ mice had a 50% reduction in platelet count (Guinard et al., 2023). We thus hypothesized that the organization of the ECM cage could contribute to the maturation process of megakaryocytes. Firstly, it appears that the number of megakaryocytes, the ploidy, and the maturation stages in *Itgb1*$^{-/-}$/*Itgb3*$^{-/-}$ mice were similar to those in the control *Pf4cre* mice (Suppl. Figure 4A). Next, we analyzed megakaryocyte localization in the bone marrow tissue. We found a significantly higher proportion of megakaryocytes that were extending intravascular fragments (i.e., intravasation) in *Itgb1*$^{-/-}$/*Itgb3*$^{-/-}$ mice (15.1 ± 2.7% of total bone marrow megakaryocytes) compared to that in *Pf4Cre* mice (2.9 ± 0.4% of total megakaryocytes). More strikingly, intact megakaryocytes were found in the blood circulation, a rare phenomenon in control mice under physiological conditions (Figure 4A).

To elucidate which of the two integrins was responsible for the observed phenotype, we employed single-knockout mice (Figure 4B). Analysis of the ECM cage revealed a trend towards decreased laminin ϒ1 density around *Itgb1*$^{-/-}$ megakaryocytes, while no notable changes were observed around *Itgb3*$^{-/-}$ cells. No statistically significant increase in intravasation events was observed in either single knock-out mouse model. This suggests a synergistic role of both integrins in regulating the megakaryocyte ECM cage and the intravasation process, potentially compensating for each other's role. Additionally, we investigate the role of GPVI, one of the two well-characterized collagen receptors in this process (Figure 4B), and no alterations in ECM cage formation or intravasation behavior were noticed, which is in agreement with previous reports (Semeniak et al., 2019).

To understand the unusual localization of circulating *Itgb1*$^{-/-}$/*Itgb3*$^{-/-}$ megakaryocyte in the bloodstream, we used intravital 2-photon microscopy imaging to describe the dynamic of the megakaryocyte behavior. Among megakaryocytes stabilized at the parasinusoidal interface, we could observe the cellular distortions of *Itgb1*$^{-/-}$/*Itgb3*$^{-/-}$ megakaryocytes and their exit of the marrow by entering the bloodstream intact (Figure 4C, movie 2). As a result, large megakaryocyte nuclei were even found in the downstream pulmonary capillaries of these mice (Figure 4D). Transmission electron microscopy (TEM) observation confirmed that intravascular *Itgb1*$^{-/-}$/*Itgb3*$^{-/-}$ megakaryocytes were similar in size and ultrastructure to those

in the stroma compartment (Figure 4E). Furthermore, no significant change in the size of the endothelial pores (*Itgb1*$^{-/-}$/*Itgb3*$^{-/-}$: 4.6 ± 0.3 µm; WT: 4.3 ± 0.4 µm) was observed, indicating the existence of alternative mechanisms.

Integrins promote megakaryocyte adhesion to the ECM components of the bone marrow

We next assessed the contribution of integrins adhesive function in megakaryocyte anchorage to ECM. Under static conditions, most *Itgb1-/-/Itgb3*$^{-/-}$ megakaryocytes did not spread and still showed a round shape on immobilized laminin, fibronectin or fibrinogen (Figure 5A). We next measured the adhesive potential of freshly isolated bone marrow megakaryocytes to test for such an adhesive role. To this end, we used a miniaturized microfluidic-based experimental model in which individual megakaryocyte detachment was tracked when exposed to a flow rate of 300s-1, similar to the flow typically found in sinusoids (Suppl. Figure 5A). *Pf4-Cre* megakaryocytes had capture yields of 59.0% on laminin, 83.6% on fibrillar fibronectin, and 82.0% on fibrinogen. Laminin exhibited the least adhesion, emphasizing the importance of the molecular composition of the said 3D ECM cage and its evident impact on the adhesion response of megakaryocytes *in vivo* (Figure 5B). *Pf4-Cre* megakaryocytes remained anchored, while *Itgb1*$^{-}$/$^{-}$/*Itgb3*$^{-}$/$^{-}$ megakaryocytes experienced higher detachment rates across various ECMs (movies 2 and 3). In line with this conclusion, we used the bone marrow explant model to study the adhesion properties of the megakaryocytes associated with their 3D ECM cage (Figure 5C). This model enabled us to quantify the physical detachment of megakaryocytes at the periphery of the explants. After 3 hours, more megakaryocytes detached from *Itgb1*$^{-/-}$/*Itgb3*$^{-/-}$ bone marrow tissue than *Pf4-Cre* explants, reaching a plateau at 6 h. These findings indicate that β1 and β3 integrins control ECM-megakaryocyte interactions in their native bone marrow microenvironment.

Collectively, our results highlight the essential roles of β1 and β3 integrins in forming 3D ECM cages around megakaryocytes and modulating their adhesion within the bone marrow, which helps stabilize the cells in their vascular niche and prevent the passage of intact megakaryocytes through the sinusoid barriers.

Cage compression via metalloproteinase inhibition affects the maturation of megakaryocytes.

Our results suggest that a weakened ECM cage promotes megakaryocyte intravasation through reduced adhesion. We, therefore, tested whether an increase in cage density also

may affect megakaryocyte functions. For that purpose, we proposed to decrease the catabolic aspect occurring in the ECM equilibrium between its synthesis and degradation. To this aim, mice were injected with batimastat (30 mg/kg) and ilomastat (20 mg/kg) for 7 days, in order to inhibit the activation of MMPs in the megakaryocyte microenvironment (Winer et al., 2018) (Supplemental Figure 6A). These mice produced platelets normally, as shown by average platelet counts (Supplemental Figure 6B). Remarkably, this treatment increased the ECM density in megakaryocyte surrounding, as evidenced by reduced fiber length and pore size (Figure 6A).

We investigated whether this denser ECM cage might affect megakaryopoiesis. Remarkably, we found a higher proportion of megakaryocytes that were significantly smaller (white arrows in Figure 6B left). To better evaluate the extent of this defect, we employed TEM. We found that 53.7 % of the megakaryocytes lacked the appropriate organization of the DMS in MMP inhibitors-treated mice, reflecting a primary failure in the cytoplasmic maturation (Stage II in Figure 6C). To determine whether MMP inhibition could directly affect megakaryocytes, we cultured primary megakaryocytes in the presence of increasing concentrations of inhibitors. We found no impact on megakaryocyte proliferation, maturation, and proplatelet formation *in vitro* (Supplement Figure 6C). These findings indicate that a dense ECM microenvironment significantly impacts megakaryocyte maturation.

An additional phenotype associated with a denser ECM environment is a significant increase in the total megakaryocyte number in MMP inhibitor-treated mice compared to the control condition (Figures 6B left and 6C middle). Moreover, immunofluorescence analysis of bone marrow sections revealed an upregulation of activated β1 integrin (Suppl. Figure 6C). These results indicate that increased ECM density may promote megakaryocyte adhesion within the congested microenvironment of the bone marrow. To further investigate this point, we quantified the number of megakaryocytes released from bone marrow explants. We observed a significant reduction in megakaryocyte egress from the bone marrow microenvironment after 6 h in MMP inhibitor-treated compared to control mice (Figure 6D). Together, these results indicate that MMPs are essential regulators of ECM homeostasis within the bone marrow, influencing megakaryocyte maturation and attachment to the vascular niche.

DISCUSSION

Physiological platelet formation relies on the strategic positioning of mature megakaryocytes at sinusoids to facilitate polarised proplatelet extension and platelet release into circulation. This study identifies a 3D ECM cage anchoring megakaryocytes to bone marrow sinusoids. This cage, composed of laminin γ1 and α4 and collagen IV fibers, extends from the basement membrane and surrounds megakaryocytes. Megakaryocyte integrin signaling and ECM proteolysis regulate its remodeling and adhesive properties. This dynamic microenvironment is crucial for megakaryocyte positioning, maturation, and intravasation into the bloodstream, representing a novel concept in understanding physiological platelet formation (Graphical Abstract, Figure 7).

In line with previous studies (Semeniak et al., 2016, Guinard et al., 2023, Larson and Watson, 2006, Malara et al., 2014), we identified the presence of collagen IV, laminin γ1, fibronectin, and fibrinogen surrounding sinusoid-associated megakaryocytes. Notably, when analyzed using immunofluorescence and transmission electron microscopy (TEM), collagen I fibers were absent under steady-state conditions. The discrepancy between our results and those reported in the literature may be attributed to differences in staining methodologies or variations in the physiological context of the bone marrow. Furthermore, our findings indicate that GPVI-deficient megakaryocytes do not display alterations in ECM cage formation, vessel association and intravasation behavior. These observations support studies showing GPVI and α2β1 integrins are not critical for megakaryocyte function, underscoring potential redundancy in ECM-receptor interactions (Semeniak et al., 2019).

Our findings identify laminin and collagen IV as the principal structural components of this ECM cage. Consistent with previous research (Abbonante et al., 2016, Susek et al., 2018, Cai et al., 2022), these ECM proteins were detected intracellularly within megakaryocytes and in stromal cells situated in their vicinity. This indicates that the ECM cage proteins may be derived from autocrine synthesis and their production by neighbouring cells.

Our findings in *Lama4*-deficient mice reveal that the ECM cage is critical for positioning megakaryocytes near sinusoids. It is established that CXCL12 is a most potent physiological chemoattractant for megakaryocytes and that the parasinusoidal location of megakaryocytes in the bone marrow is mediated by the CXCL12/CXCR4 interaction (Hamada et al., 1998, Wang et al., 2019). Other chemoattractive factors also include fibroblast growth factor 4 (FGF4) (Avecilla et al., 2004) and von Willebrand factor (VWF) (Ouzegdouh et al., 2018). Besides its

potential role as a reservoir of such growth factors, we show that the ECM cage is also a crucial element in maintaining megakaryocytes in the proximity of sinusoids, which is essential for their optimal maturation and efficient platelet production. We also find the persistent presence of this ECM cage throughout megakaryocyte maturation, supporting previous findings that megakaryocyte development occurs primarily at the sinusoid (Stegner et al., 2017, Lichtman et al., 1978). Further research is required to clarify whether the ECM cage plays also a role in retaining immature megakaryocytes within the bone marrow until they are ready for platelet production or anchoring residual pyrenocytes at the bone marrow-blood interface to prevent their release into the circulation.

Our study highlights the indispensable roles of β1 and β3 integrins in maintaining megakaryocyte stability within the vascular niche. We demonstrate that these integrins are crucial for two fundamental processes: (1) the building of the 3D ECM cages, and (2) the ECM-mediated adhesion mechanisms to the vascular niche. Our work further demonstrates that in *Itgb1*$^{-/-}$/*Itgb3*$^{-/-}$ mice, intact megakaryocytes can enter the general circulation. Importantly, circulating megakaryocytes have also been observed in humans during emergency megakaryopoiesis, such as in cases of infectious diseases, inflammatory conditions, and following cardiopulmonary bypass procedures (Gelon et al., 2022, Puhm et al., 2023, Rapkiewicz et al., 2020, Frydman et al., 2023). These circulating megakaryocytes have been implicated in thrombotic complications, underscoring the importance of integrin signaling-dependent mechanisms regulating megakaryocyte retention and release.

MMPs profoundly influence megakaryocyte maturation and their association with the vascular niche by modulating the density of ECM cage architecture. This finding highlights the dynamic nature of the bone marrow microenvironment and its impact on megakaryopoiesis. Dysregulation of ECM production, often associated with bone marrow pathologies, can lead to its uncontrolled accumulation. In myelofibrosis, for instance, megakaryocytes secrete transforming growth factor-β1 (TGF-β1) which stimulates excessive ECM production by stromal cells (Abbonante et al., 2016). This pathological ECM accumulation leads to abnormally smaller megakaryocytes that exhibit reduced platelet production (Gianelli et al., 2023, Malara et al., 2018a, Sarachakov et al., 2023). Likewise, we observed smaller and immature megakaryocytes retained in the constrained ECM microenvironment of the bone marrow, associated with an upregulation of activated β1 integrin in treated mice. Interestingly, previous research by K. Hoffmeister's group has demonstrated that proper

megakaryocyte localization at the sinusoids depends on β1 integrin glycosylation. Specifically, the absence of galactosylation in β4galt1-/- megakaryocytes leads to hyperactivity of β1 integrin, which negatively impacts the formation of the demarcation membrane system (DMS) and the platelet-forming process (Giannini et al., 2020). Our study extends these findings by revealing the coordinated interplay between integrin-mediated signaling and MMP proteolysis, working together to tightly regulate the density and cross-linking properties of the ECM cage and thereby control megakaryocyte maturation at the bone marrow-blood interface. Intriguingly, despite these effects on megakaryocyte maturation, we observed no significant changes in circulating platelet counts. This needs further investigation. A possible explanation could be that the proteolytic treatment affected platelet clearance mechanisms, counteracting its impact on megakaryocyte maturation. The increased number of immature megakaryocytes might also contribute to platelet formation.

An increased ECM density creates a stiffer microenvironment, which could directly influence cell growth and maturation processes (Barriga et al., 2018, Dolega et al., 2021). The mechanical properties of the ECM, particularly its stiffness, have emerged as critical environmental determinants of megakaryocyte development and function (Aguilar et al., 2016, Leiva et al., 2018, Abbonante et al., 2017, Guinard et al., 2023). Notably, megakaryocytes possess mechanosensing capabilities, primarily mediated by the β3 integrin subunit, enabling them to detect and respond to changes in substrate stiffness (Guinard et al., 2023, Abbonante et al., 2024). The assembly of extracellular matrix (ECM) fibronectin around megakaryopoiesis involves a more complex interplay of integrins, with both β1 and β3 integrins playing essential roles in fibrillogenesis (Guinard et al., 2023). This cooperative relationship appears to be conserved across various cell types (De Mets et al., 2019, Kyumurkov et al., 2023, Attieh et al., 2017). This may explain why the deletion of both integrins is required to affect the 3D ECM cage and megakaryocyte behavior significantly. We can not exclude that other ECM ligands of β3 integrins, such as fibronectin, may contribute to the organization of collagen IV and laminin, influencing the overall architecture of the vascular niche (Zeng et al., 2018, Petito and Gresele, 2024, Yang et al., 2022). Indeed, it is known that the fibronectin matrix favors the deposition of other ECM proteins, such as collagens IV and various other glycoproteins (Saunders and Schwarzbauer, 2019). This hypothesis underscores the need for further investigation into the spatio-temporal dynamics of ECM component assembly in the megakaryocyte vascular niche.

Overall, the current study demonstrates how the complexity of the 3D ECM microenvironment determines the fate of megakaryocytes in their vascular niche. It highlights the importance of the ECM cage as an active physical scaffold that precisely regulates megakaryocyte positioning and maturation. Maintaining the integrity of the 3D ECM cage and modelling the complex physical constraints that occur in the parasinusoidal region will be important topics for future studies on platelet biogenesis under physiological and stress conditions, particularly in inflammation, where there is an increased incidence of thrombus formation caused by an excess of circulating megakaryocytes.

MATERIAL and METHODS

Animals. We used wild type (WT) mice (C57BL/6J from C. River, L'Arbesle, France), Itgb1$^{-/-}$/Itgb3$^{-/-}$ double knock out mice and Pf4cre mice aged 10 to 15 weeks. Pf4cre mice expressed the Cre recombinase under the control of the Pf4 promoter. The β1$^{fl/fl}$ (Potocnik et al., 2000) and β3$^{fl/fl}$ (Morgan et al., 2010) mice were crossed with mice expressing the Cre recombinase under the control of the Pf4 promoter to obtain inactivation in the MK lineage. *Itgb1$^{-/-}$/Itgb3$^{-/-}$* double knock out (KO) mice were crosses of the two single KO lines, as described in Guinard et al., 2023. *GPVI $^{-/-}$* mice and *Lama4$^{-/-}$* CD45.2 C57BL/6J mice were from Nieswandt and Qian labs (Cai et al., 2022, Bender et al., 2011). All animal studies were approved by the French legislation for animal experimentation and in accordance with the guide for the care and use of laboratory animals as defined by the European laws (Animal Facility Agreement C-67-482-10).

Chemicals. Dimethyl sulfoxide (2438), bovine serum albumin (900.011), saponin (47036), Triton X-100 (T8787), fibrinogen and batimastat (SML0041) (Sigma-Aldrich, Rueil-Malmaison, France), Ilomastat (GM6001, HY-15768) (MedChemExpress, Clinisciences, France), Dulbecco's modified Eagle's medium (DMEM), penicillin, streptomycin, and glutamine (Invitrogen , Cergy-Pontoise, France), Gelatin-Oregon Green 488 conjugate (G-13186) (Life Technologies, COUNTRY?), Laminin 511 recombinant (Biolamina) and fibronectin from human plasma from (341635, Calbiochem) were used in this study.

Antibodies. See Table 1 in "Data Supplements" for details.

Preparation of BM and megakaryocytes. Our technique excludes the decalcification step, which is known to destroy selective epitopes and may lead to artifacts. In this study, murine BM was obtained by flushing the femurs of mice with PBS followed by fixation. Megakaryocytes were dissociated using a 21G needle and filtered through a 40 µm Millipore filter. The filter was then rinsed in DMEM + 1% fœtal bovine serum, and the isolated megakaryocytes were adjusted to 300 cells/ml in the same medium.

2D confocal microscopy on BM cryosections. BM cryosections from WT mice were used to study the ECM composition and distribution of sinusoid-associated megakaryocytes. BM was

fixed in a mix of 2% paraformaldehyde-0.2% glutaraldehyde, frozen in liquid nitrogen, and cut as described (Eckly et al., 2020). For immunofluorescence staining, 250 nm-thick cryosections were labeled with primary antibodies and conjugated-second antibodies of the appropriate species and DAPI, as reported in Table 1. They were examined under a confocal microscope (TCS SP8, Leica) using the 63x objective with a numerical zoom of 4 (pixel size: 0.09µm). The BM specimens from 3 mice were examined under identical conditions, using constant exposure and the same irrelevant antibodies. No fluorescence was detected using isotype-specific control IgG.

3D confocal analysis on BM vibratome sections. Whole-mount BM preparations were used to investigate i) the localization of megakaryocytes in the BM and the lung and ii) the spatial organization of ECM around sinusoid-associated megakaryocytes. Megakaryocytes were classified based on their maturation stage: stage I (presence of granules, no clear DMS visible), stage II (developing DMS not yet organized), and stage III (DMS organized in platelet territories). Mice from each genotype were analyzed and image acquisitions were performed in a blinded manner.

For megakaryocyte localization, sections of femurs or lungs fixed in 2% paraformaldehyde and 0.2% glutaraldehyde, with a thickness of 250 µm, were incubated with FABP4 overnight. This was followed by overnight staining with Alexa 568-conjugated anti-GPIbβ antibody and Alexa 488 Donkey anti-Goat for FABP4. Finally, Hoechst 33342 was used for counterstaining for 10 minutes. The fluorescently labeled tissue was placed cut-face down into incubation chambers and mounted with Mowiol mounting solution. The Leica SP8 confocal microscope was used to collect a series of x-y-z images. The images were typically 194x194 µm x-y size and were collected along the z-axis at 1 µm step size through 50 µm of BM tissue. The 40x objective with a numerical zoom of 4 (pixel size: 0.142 µm) was used. The lung was imaged using an x63 objective with a 2.5 digital zoom (pixel size: 0.145 µm).

To perform 3D ECM analysis, 250 µm-thick vibratome sections were fixed in 4% PFA and embedded in 4% agarose, incubated overnight at 4°C with an array of antibodies that targeted matrix proteins (laminin, type IV collagen, fibronectin, and fibrinogen), and were followed by the corresponding secondary antibodies and Hoechst 33342 counterstaining. Series of x-y-z images of typically 46.13*46.13 µm x-y size were collected along the z-axis at 1 µm step size through 15-35 µm of sinusoid-associated megakaryocytes, using the 63x objective with a

numerical zoom of 4 (pixel size: 0.09) from a Leica SP8 confocal microscope. For quantitative spatial analysis of ECM around megakaryocytes, the observations have been made on z-stacks as described by *Voisin et al. (Voisin et al., 2010).* The fluorescence was delineated on the maximum z-stack projection of half a megakaryocyte using Image J software.

Image processing to perform quantitative analyses of fluorescence profiles, mesh diameter, and fiber length are explained in Suppl. Figure 7. Briefly, a binary threshold mask (0 for the background and 1 for the ECM network, threshold to reduce signal noise) was generated from the channel showing labeled collagen or laminin. The mask was then applied to the channel showing megakaryocytes, resulting in an image that corresponded to only an active ECM signal that colocalized with megakaryocytes. The mask was then applied to the collagen/laminin channel to determine the amount of fluorescent ECM within the mask. This enabled the determination of the cell area and the elimination of the signal outside the mask.

Intravital imaging. *Pf4cre* and *Itgb1*$^{-/-}$*/Itgb3-/-* mice underwent intravital imaging. To visualize megakaryocytes and sinusoids, an AF488-conjugated anti-GPIX antibody derivative and Texas Red dextran 70kDa were intravenously injected, respectively. The skull bone marrow was observed using two-photon microscopy, following the procedure described in reference (Bornert et al., 2021). The anesthetized mice were monitored for a maximum of 6 hours, during which one to four proplatelets were recorded. Two regions of interest were analyzed, each composed of 3 images (xyz = 1320 µm*1320 µm*100 µm, total volume/ROI = 0.17 µm3, pixel size = 0.867 µm at obj HC FLUOTAR L 25x/0.95 WATER zoom x1). A total of 130 megakaryocytes *PF4cre* vs. 130 megakaryocytes *Itgb1*$^{-/-}$*/Itgb3*$^{-/-}$ were analyzed and the results are expressed in %.

Electron microscopy. For Transmission electron microscopy, BM was fixed in 2.5% glutaraldehyde and embedded in Epon as described (Scandola et al., 2021). Transversal thin sections of the entire BM were cut and examined under a CM120 TEM (FEI). The number of BM megakaryocytes was counted per surface unit (s.u., 12,945 µm2). The observations from three independent mice were averaged.

For SEM, native BM megakaryocytes were allowed to adhere to a surface coated with 300 µg/ml fibronectin, 100 µg/ml fibrinogen, or 50 µg/ml laminin 511. After gentle agitation to

detach non-adherent cells, the remaining adherent cells were fixed in 2.5 % glutaraldehyde, dehydrated, attached to stubs, sputter coated, and examined under a Helios NanoLab microscope at 5kV (ThermoFisher, Eindhoven, The Netherlands). Adherent megakaryocytes where counted and classified as spreading or round cells. The results were obtained by the average from three independent mice.

Flow cytometry. For the ploidy analysis of the native megakaryocytes, mouse femurs, tibias, and iliac crests were harvested, cut into small fragments, and incubated in a PBS-collagenase-dispase mix (at 3 mg/mL and 4 mg/mL, 5mL/mouse respectively) for 30 min at 37°C. Then, the tube was filled with PBS-2% NCS to stop the collagenase, and the supernatant was 70 µm filtered to eliminate the bone fragments. After red cell lysis, the freshly isolated BMs were washed in PBS-2% NCS and stained with anti-CD41 and anti-CD42c antibodies and Hoechst. Anti Gr-1, B220, F4/80, and TER119 probes were used as a negative control to exclude granulocytes, B lymphocytes, macrophages, and erythrocytes from the total BM suspension. The freshly isolated megakaryocytes were identified as a CD41/CD42c positive cell population and ploidy analysis was performed using Hoechst 33342. The results are representative of three independent experiments.

Microfluidic experiments The PDMS microfluidic chamber channels were assembled and connected to a peristaltic pump, as described (Osmani et al., 2021). The channels were washed with PBS for 5 min and coated with laminin 511 (50 µg/ml), fibrillar fibronectin (300 µg/ml), or fibrinogen (100 µg/ml) overnight at 4°C, followed by a blocking stage with human serum albumin (1 %) for 30 min at RT. To produce fibrillar fibronectin, we use the method of mechanical stretching as described in Maurer et al, (Maurer et al., 2015). Freshly isolated megakaryocytes were seeded at a concentration of 30 cells /µL per channel and incubated for 15 min – 45 min at 37 °C with 5 % CO_2. In previous work, the seeding time was determined with capture efficiencies of over 80 % for Pf4cre megakaryocytes (Suppl. Figure 4B). The channels were then perfused under a flow of 300 µm/s and the megakaryocyte behavior was monitored in real-time, for 1 min, using a Leica DMI8 microscope (x20) equipped with a CMOS Camera (Hamamatsu ORCA fusion). Megakaryocyte capture yield was measured by quantifying the number of adherent megakaryocytes before and after flow induction (expressed as a percentage) on an average of 20 stage positions (n= 50 megakaryocytes

analyzed/test). The results are an average of three independent experiments, the values were expressed as a mean ± sem.

Megakaryocyte emigration from bone marrow explants. Preparation of BM explants was performed as described in Guinard et al., 2021 (Guinard et al., 2021). Briefly, BM from femur *Pf4cre* or *Itgb1*$^{-/-}$/*Itgb3*$^{-/-}$ mice were flushed and ten 0.5 mm-thick sections were placed in an incubation chamber. Megakaryocytes at the periphery of the explants were counted under an inverted phase contrast microscope coupled to a video camera (DMI8 Leica microscope, 40x objective). A motorized multiposition stage (in *x, y*, *z*) was used, and an average of 100 stages positions showing megakaryocytes was followed. Results are expressed as the number of total emigrating megakaryocytes at the indicated time points. In each case, a minimum of six independent experiments were performed. Mice from each genotypes were analyzed and image acquisitions were performed in a blinded manner.

Effects of MMP inhibition. Batimastat plus ilomastat treatment was tested for their potential impact on the ECM in the microenvironment of the megakaryocyte vascular niche. Mice were treated daily with a protease inhibitor cocktail (Batimastat at 30 mg/kg + Ilomastat at 50 mg/kg) or vehicle (DMSO) for 7 consecutive days (Gui et al., 2018, Pielecka-Fortuna et al., 2015). The platelet count was monitored every two days. On the eighth day, the mice were sacrificed, and their BM was collected for analysis of ECM organization and megakaryocyte behavior, as explained in the 3D confocal analysis on BM vibratome sections.

Gelatin degradation assay. Coverslips were coated with Oregon green gelatin, and fixed with 0.5% glutaraldehyde for 20 min at RT. After washing three times with PBS, cells were seeded on coated coverslips and incubated for 6 h before fixation and staining.

Statistics. All values are reported as the mean ± sem. n= number of megakaryocytes studied. Statistical analyses were performed with PrismGraphpad software (La Jolla, CA, USA). For group comparison, data were tested for Gaussian distribution. Then, a Student t-test (Gaussian) or Mann-Whitney U test (non-Gaussian) were used to compare individual groups; multiple groups were compared by one-way ANOVA followed by Bonferroni post-test, with a

threshold of significance of 5%. P-values <0.05 were considered statistically significant. *P<0.05; **P<0.01; ***P<0.001.

CONTRIBUTIONS

C.M and C.S performed experiments, analyzed data, and contributed to the writing of the revised manuscript; JY.R, F.P, E.J-B, N.O, L.M, A.M. and A.B performed experiments, analyzed data, and commented on the manuscript; J.G, N.O, C.Q, F.B, and C.L provided vital reagents and commented on the manucript; R.P., O.D, and M.L contributed to the writing of the manuscript; and A.E designed and supervised research, analyzed data, and wrote the manuscript

Acknowledgments

We wish to thank Ketty Knez-Hippert (EFS-GEST) for excellent expert technical assistance. This work was supported by ARMESA (Association de Recherche et Développement en Médecine et Santé Publique) and by ANR Grant MegaPod (ANR-22-CE14-0029). The authors thank Pr. B. Nieswandt for providing GPVI knock-out mice.

Discosure of conflicts of interest

The authors have no conflicts of interests to declare

REFERENCES

ABBONANTE, V., CHITALIA, V., ROSTI, V., LEIVA, O., MATSUURA, S., BALDUINI, A. & RAVID, K. 2017. Upregulation of lysyl oxidase and adhesion to collagen of human megakaryocytes and platelets in primary myelofibrosis. *Blood,* 130**,** 829-831.

ABBONANTE, V., DI BUDUO, C. A., GRUPPI, C., MALARA, A., GIANELLI, U., CELESTI, G., ANSELMO, A., LAGHI, L., VERCELLINO, M., VISAI, L., IURLO, A., MORATTI, R., BAROSI, G., ROSTI, V. & BALDUINI, A. 2016. Thrombopoietin/TGF-beta1 Loop Regulates Megakaryocyte Extracellular Matrix Component Synthesis. *Stem Cells,* 34**,** 1123-33.

ABBONANTE, V., KARKEMPETZAKI, A. I., LEON, C., KRISHNAN, A., HUANG, N., DI BUDUO, C. A., CATTANEO, D., WARD, C. M., MATSUURA, S., GUINARD, I., WEBER, J., DE ACUTIS, A., VOZZI, G., IURLO, A., RAVID, K. & BALDUINI, A. 2024. Newly identified roles for PIEZO1 mechanosensor in controlling normal megakaryocyte development and in primary myelofibrosis. *Am J Hematol,* 99**,** 336-349.

AGUILAR, A., PERTUY, F., ECKLY, A., STRASSEL, C., COLLIN, D., GACHET, C., LANZA, F. & LEON, C. 2016. Importance of environmental stiffness for megakaryocyte differentiation and proplatelet formation. *Blood,* 128**,** 2022-2032.

ATTIEH, Y., CLARK, A. G., GRASS, C., RICHON, S., POCARD, M., MARIANI, P., ELKHATIB, N., BETZ, T., GURCHENKOV, B. & VIGNJEVIC, D. M. 2017. Cancer-associated fibroblasts lead tumor invasion through integrin-beta3-dependent fibronectin assembly. *J Cell Biol,* 216**,** 3509-3520.

AVECILLA, S. T., HATTORI, K., HEISSIG, B., TEJADA, R., LIAO, F., SHIDO, K., JIN, D. K., DIAS, S., ZHANG, F., HARTMAN, T. E., HACKETT, N. R., CRYSTAL, R. G., WITTE, L., HICKLIN, D. J., BOHLEN, P., EATON, D., LYDEN, D., DE SAUVAGE, F. & RAFII, S. 2004. Chemokine-mediated interaction of hematopoietic progenitors with the bone marrow vascular niche is required for thrombopoiesis. *Nat Med,* 10**,** 64-71.

BALDUINI, A., PALLOTTA, I., MALARA, A., LOVA, P., PECCI, A., VIARENGO, G., BALDUINI, C. L. & TORTI, M. 2008. Adhesive receptors, extracellular proteins and myosin IIA orchestrate proplatelet formation by human megakaryocytes. *J Thromb Haemost,* 6**,** 1900-7.

BARRIGA, E. H., FRANZE, K., CHARRAS, G. & MAYOR, R. 2018. Tissue stiffening coordinates morphogenesis by triggering collective cell migration in vivo. *Nature,* 554**,** 523-527.

BENDER, M., HAGEDORN, I. & NIESWANDT, B. 2011. Genetic and antibody-induced glycoprotein VI deficiency equally protects mice from mechanically and FeCl(3) -induced thrombosis. *J Thromb Haemost,* 9**,** 1423-6.

BORNERT, A., BOSCHER, J., PERTUY, F., ECKLY, A., STEGNER, D., STRASSEL, C., GACHET, C., LANZA, F. & LEON, C. 2021. Cytoskeletal-based mechanisms differently regulate in vivo and in vitro proplatelet formation. *Haematologica,* 106**,** 1368-1380.

BOSCHER, J., GUINARD, I., ECKLY, A., LANZA, F. & LEON, C. 2020. Blood platelet formation at a glance. *J Cell Sci,* 133.

CAI, H., KONDO, M., SANDHOW, L., XIAO, P., JOHANSSON, A. S., SASAKI, T., ZAWACKA-PANKAU, J., TRYGGVASON, K., UNGERSTEDT, J., WALFRIDSSON, J., EKBLOM, M. & QIAN, H. 2022. Critical role of Lama4 for hematopoiesis regeneration and acute myeloid leukemia progression. *Blood,* 139**,** 3040-3057.

DE METS, R., WANG, I., BALLAND, M., ODDOU, C., MOREAU, P., FOURCADE, B., ALBIGES-RIZO, C., DELON, A. & DESTAING, O. 2019. Cellular tension encodes local Src-dependent differential beta(1) and beta(3) integrin mobility. *Mol Biol Cell,* 30**,** 181-190.

DOLEGA, M. E., MONNIER, S., BRUNEL, B., JOANNY, J. F., RECHO, P. & CAPPELLO, G. 2021. Extracellular matrix in multicellular aggregates acts as a pressure sensor controlling cell proliferation and motility. *Elife,* 10.

ECKLY, A., SCANDOLA, C., OPRESCU, A., MICHEL, D., RINCKEL, J. Y., PROAMER, F., HOFFMANN, D., RECEVEUR, N., LEON, C., BEAR, J. E., GHALLOUSSI, D., HAROUSSEAU, G., BERGMEIER, W.,

LANZA, F., GAITS-IACOVONI, F., DE LA SALLE, H. & GACHET, C. 2020. Megakaryocytes use in vivo podosome-like structures working collectively to penetrate the endothelial barrier of bone marrow sinusoids. *J Thromb Haemost,* 18**,** 2987-3001.

ELIADES, A., PAPADANTONAKIS, N., BHUPATIRAJU, A., BURRIDGE, K. A., JOHNSTON-COX, H. A., MIGLIACCIO, A. R., CRISPINO, J. D., LUCERO, H. A., TRACKMAN, P. C. & RAVID, K. 2011. Control of megakaryocyte expansion and bone marrow fibrosis by lysyl oxidase. *J Biol Chem,* 286**,** 27630-8.

FRYDMAN, G. H., ELLETT, F., JORGENSEN, J., MARAND, A. L., ZUKERBERG, L., SELIG, M. K., TESSIER, S. N., WONG, K. H. K., OLALEYE, D., VANDERBURG, C. R., FOX, J. G., TOMPKINS, R. G. & IRIMIA, D. 2023. Megakaryocytes respond during sepsis and display innate immune cell behaviors. *Front Immunol,* 14**,** 1083339.

GELON, L., FROMONT, L. & LEFRANCAIS, E. 2022. Occurrence and role of lung megakaryocytes in infection and inflammation. *Front Immunol,* 13**,** 1029223.

GIANELLI, U., THIELE, J., ORAZI, A., GANGAT, N., VANNUCCHI, A. M., TEFFERI, A. & KVASNICKA, H. M. 2023. International Consensus Classification of myeloid and lymphoid neoplasms: myeloproliferative neoplasms. *Virchows Arch,* 482**,** 53-68.

GIANNINI, S., LEE-SUNDLOV, M. M., RIVADENEYRA, L., DI BUDUO, C. A., BURNS, R., LAU, J. T., FALET, H., BALDUINI, A. & HOFFMEISTER, K. M. 2020. beta4GALT1 controls beta1 integrin function to govern thrombopoiesis and hematopoietic stem cell homeostasis. *Nat Commun,* 11**,** 356.

GUI, P., BEN-NEJI, M., BELOZERTSEVA, E., DALENC, F., FRANCHET, C., GILHODES, J., LABROUSSE, A., BELLARD, E., GOLZIO, M., POINCLOUX, R., MARIDONNEAU-PARINI, I. & LE CABEC, V. 2018. The Protease-Dependent Mesenchymal Migration of Tumor-Associated Macrophages as a Target in Cancer Immunotherapy. *Cancer Immunol Res,* 6**,** 1337-1351.

GUINARD, I., LANZA, F., GACHET, C., LEON, C. & ECKLY, A. 2021. Proplatelet Formation Dynamics of Mouse Fresh Bone Marrow Explants. *J Vis Exp*.

GUINARD, I., NGUYEN, T., BRASSARD-JOLLIVE, N., WEBER, J., RUCH, L., REININGER, L., BROUARD, N., ECKLY, A., COLLIN, D., LANZA, F. & LEON, C. 2023. Matrix stiffness controls megakaryocyte adhesion, fibronectin fibrillogenesis, and proplatelet formation through Itgbeta3. *Blood Adv,* 7**,** 4003-4018.

HAMADA, T., MOHLE, R., HESSELGESSER, J., HOXIE, J., NACHMAN, R. L., MOORE, M. A. & RAFII, S. 1998. Transendothelial migration of megakaryocytes in response to stromal cell-derived factor 1 (SDF-1) enhances platelet formation. *J Exp Med,* 188**,** 539-48.

KYUMURKOV, A., BOUIN, A. P., BOISSAN, M., MANET, S., BASCHIERI, F., PROPONNET-GUERAULT, M., BALLAND, M., DESTAING, O., REGENT-KLOECKNER, M., CALMEL, C., NICOLAS, A., WAHARTE, F., CHAVRIER, P., MONTAGNAC, G., PLANUS, E. & ALBIGES-RIZO, C. 2023. Force tuning through regulation of clathrin-dependent integrin endocytosis. *J Cell Biol,* 222.

LARSON, M. K. & WATSON, S. P. 2006. Regulation of proplatelet formation and platelet release by integrin alpha IIb beta3. *Blood,* 108**,** 1509-14.

LEIVA, O., LEON, C., KAH NG, S., MANGIN, P., GACHET, C. & RAVID, K. 2018. The role of extracellular matrix stiffness in megakaryocyte and platelet development and function. *Am J Hematol,* 93**,** 430-441.

LICHTMAN, M. A., CHAMBERLAIN, J. K., SIMON, W. & SANTILLO, P. A. 1978. Parasinusoidal location of megakaryocytes in marrow: a determinant of platelet release. *Am J Hematol,* 4**,** 303-12.

MALARA, A., ABBONANTE, V., ZINGARIELLO, M., MIGLIACCIO, A. & BALDUINI, A. 2018a. Megakaryocyte Contribution to Bone Marrow Fibrosis: many Arrows in the Quiver. *Mediterr J Hematol Infect Dis,* 10**,** e2018068.

MALARA, A., CURRAO, M., GRUPPI, C., CELESTI, G., VIARENGO, G., BURACCHI, C., LAGHI, L., KAPLAN, D. L. & BALDUINI, A. 2014. Megakaryocytes contribute to the bone marrow-matrix environment by expressing fibronectin, type IV collagen, and laminin. *Stem Cells,* 32**,** 926-37.

MALARA, A., LIGI, D., DI BUDUO, C. A., MANNELLO, F. & BALDUINI, A. 2018b. Sub-Cellular Localization of Metalloproteinases in Megakaryocytes. *Cells,* 7.

MAURER, E., SCHAFF, M., RECEVEUR, N., BOURDON, C., MERCIER, L., NIESWANDT, B., DUBOIS, C., JANDROT-PERRUS, M., GOETZ, J. G., LANZA, F., GACHET, C. & MANGIN, P. H. 2015. Fibrillar cellular fibronectin supports efficient platelet aggregation and procoagulant activity. *Thromb Haemost,* 114**,** 1175-88.

MORGAN, E. A., SCHNEIDER, J. G., BARONI, T. E., ULUCKAN, O., HELLER, E., HURCHLA, M. A., DENG, H., FLOYD, D., BERDY, A., PRIOR, J. L., PIWNICA-WORMS, D., TEITELBAUM, S. L., ROSS, F. P. & WEILBAECHER, K. N. 2010. Dissection of platelet and myeloid cell defects by conditional targeting of the beta3-integrin subunit. *FASEB J,* 24**,** 1117-27.

OPRESCU, A., MICHEL, D., ANTKOWIAK, A., VEGA, E., VIAUD, J., COURTNEIDGE, S. A., ECKLY, A., DE LA SALLE, H., CHICANNE, G., LEON, C., PAYRASTRE, B. & GAITS-IACOVONI, F. 2022. Megakaryocytes form linear podosomes devoid of digestive properties to remodel medullar matrix. *Sci Rep,* 12**,** 6255.

OSMANI, N., FOLLAIN, G., GENSBITTEL, V., GARCIA-LEON, M. J., HARLEPP, S. & GOETZ, J. G. 2021. Probing Intravascular Adhesion and Extravasation of Tumor Cells with Microfluidics. *Methods Mol Biol,* 2294**,** 111-132.

OUZEGDOUH, Y., CAPRON, C., BAUER, T., PUYMIRAT, E., DIEHL, J. L., MARTIN, J. F. & CRAMER-BORDE, E. 2018. The physical and cellular conditions of the human pulmonary circulation enable thrombopoiesis. *Exp Hematol,* 63**,** 22-27 e3.

PETITO, E. & GRESELE, P. 2024. Immune attack on megakaryocytes in immune thrombocytopenia. *Res Pract Thromb Haemost,* 8**,** 102345.

PIELECKA-FORTUNA, J., KALOGERAKI, E., FORTUNA, M. G. & LOWEL, S. 2015. Optimal level activity of matrix metalloproteinases is critical for adult visual plasticity in the healthy and stroke-affected brain. *Elife,* 5**,** e11290.

POTOCNIK, A. J., BRAKEBUSCH, C. & FASSLER, R. 2000. Fetal and adult hematopoietic stem cells require beta1 integrin function for colonizing fetal liver, spleen, and bone marrow. *Immunity,* 12**,** 653-63.

PUHM, F., LAROCHE, A. & BOILARD, E. 2023. Diversity of Megakaryocytes. *Arterioscler Thromb Vasc Biol,* 43**,** 2088-2098.

RADLEY, J. M. & HALLER, C. J. 1983. Fate of senescent megakaryocytes in the bone marrow. *Br J Haematol,* 53**,** 277-87.

RAPKIEWICZ, A. V., MAI, X., CARSONS, S. E., PITTALUGA, S., KLEINER, D. E., BERGER, J. S., THOMAS, S., ADLER, N. M., CHARYTAN, D. M., GASMI, B., HOCHMAN, J. S. & REYNOLDS, H. R. 2020. Megakaryocytes and platelet-fibrin thrombi characterize multi-organ thrombosis at autopsy in COVID-19: A case series. *EClinicalMedicine,* 24**,** 100434.

SABRI, S., JANDROT-PERRUS, M., BERTOGLIO, J., FARNDALE, R. W., MAS, V. M., DEBILI, N. & VAINCHENKER, W. 2004. Differential regulation of actin stress fiber assembly and proplatelet formation by alpha2beta1 integrin and GPVI in human megakaryocytes. *Blood,* 104**,** 3117-25.

SARACHAKOV, A., VARLAMOVA, A., SVEKOLKIN, V., POLYAKOVA, M., VALENCIA, I., UNKENHOLZ, C., PANNELLINI, T., GALKIN, I., OVCHAROV, P., TABAKOV, D., POSTOVALOVA, E., SHIN, N., SETHI, I., BAGAEV, A., ITKIN, T., CRANE, G., KLUK, M., GEYER, J., INGHIRAMI, G. & PATEL, S. 2023. Spatial mapping of human hematopoiesis at single-cell resolution reveals aging-associated topographic remodeling. *Blood,* 142**,** 2282-2295.

SAUNDERS, J. T. & SCHWARZBAUER, J. E. 2019. Fibronectin matrix as a scaffold for procollagen proteinase binding and collagen processing. *Mol Biol Cell,* 30**,** 2218-2226.

SCANDOLA, C., LANZA, F., GACHET, C. & ECKLY, A. 2021. In Situ Exploration of Murine Megakaryopoiesis using Transmission Electron Microscopy. *J Vis Exp*.

SEMENIAK, D., FABER, K., OFTERING, P., MANUKJAN, G. & SCHULZE, H. 2019. Impact of Itga2-Gp6-double collagen receptor deficient mice for bone marrow megakaryocytes and platelets. *PLoS One,* 14**,** e0216839.

SEMENIAK, D., KULAWIG, R., STEGNER, D., MEYER, I., SCHWIEBERT, S., BOSING, H., ECKES, B., NIESWANDT, B. & SCHULZE, H. 2016. Proplatelet formation is selectively inhibited by collagen type I through Syk-independent GPVI signaling. *J Cell Sci,* 129**,** 3473-84.

STEGNER, D., VANEEUWIJK, J. M. M., ANGAY, O., GORELASHVILI, M. G., SEMENIAK, D., PINNECKER, J., SCHMITHAUSEN, P., MEYER, I., FRIEDRICH, M., DUTTING, S., BREDE, C., BEILHACK, A., SCHULZE, H., NIESWANDT, B. & HEINZE, K. G. 2017. Thrombopoiesis is spatially regulated by the bone marrow vasculature. *Nat Commun,* 8**,** 127.

STONE, A. P., NASCIMENTO, T. F. & BARRACHINA, M. N. 2022. The bone marrow niche from the inside out: how megakaryocytes are shaped by and shape hematopoiesis. *Blood,* 139**,** 483-491.

SUSEK, K. H., KORPOS, E., HUPPERT, J., WU, C., SAVELYEVA, I., ROSENBAUER, F., MULLER-TIDOW, C., KOSCHMIEDER, S. & SOROKIN, L. 2018. Bone marrow laminins influence hematopoietic stem and progenitor cell cycling and homing to the bone marrow. *Matrix Biol,* 67**,** 47-62.

VILLENEUVE, J., BLOCK, A., LE BOUSSE-KERDILES, M. C., LEPREUX, S., NURDEN, P., RIPOCHE, J. & NURDEN, A. T. 2009. Tissue inhibitors of matrix metalloproteinases in platelets and megakaryocytes: a novel organization for these secreted proteins. *Exp Hematol,* 37**,** 849-56.

VOISIN, M. B., PROBSTL, D. & NOURSHARGH, S. 2010. Venular basement membranes ubiquitously express matrix protein low-expression regions: characterization in multiple tissues and remodeling during inflammation. *Am J Pathol,* 176**,** 482-95.

WANG, M., FENG, R., ZHANG, J. M., XU, L. L., FENG, F. E., WANG, C. C., WANG, Q. M., ZHU, X. L., HE, Y., XUE, J., FU, H. X., LV, M., KONG, Y., CHANG, Y. J., XU, L. P., LIU, K. Y., HUANG, X. J. & ZHANG, X. H. 2019. Dysregulated megakaryocyte distribution associated with nestin(+) mesenchymal stem cells in immune thrombocytopenia. *Blood Adv,* 3**,** 1416-1428.

WINER, A., ADAMS, S. & MIGNATTI, P. 2018. Matrix Metalloproteinase Inhibitors in Cancer Therapy: Turning Past Failures Into Future Successes. *Mol Cancer Ther,* 17**,** 1147-1155.

YANG, X., CHITALIA, S. V., MATSUURA, S. & RAVID, K. 2022. Integrins and their role in megakaryocyte development and function. *Exp Hematol,* 106**,** 31-39.

ZENG, D. F., CHEN, F., WANG, S., CHEN, S. L., XU, Y., SHEN, M. Q., DU, C. H., WANG, C., KONG, P. Y., CHENG, T. M., SU, Y. P. & WANG, J. P. 2018. Autoantibody against integrin alpha(v) beta(3) contributes to thrombocytopenia by blocking the migration and adhesion of megakaryocytes. *J Thromb Haemost,* 16**,** 1843-1856.

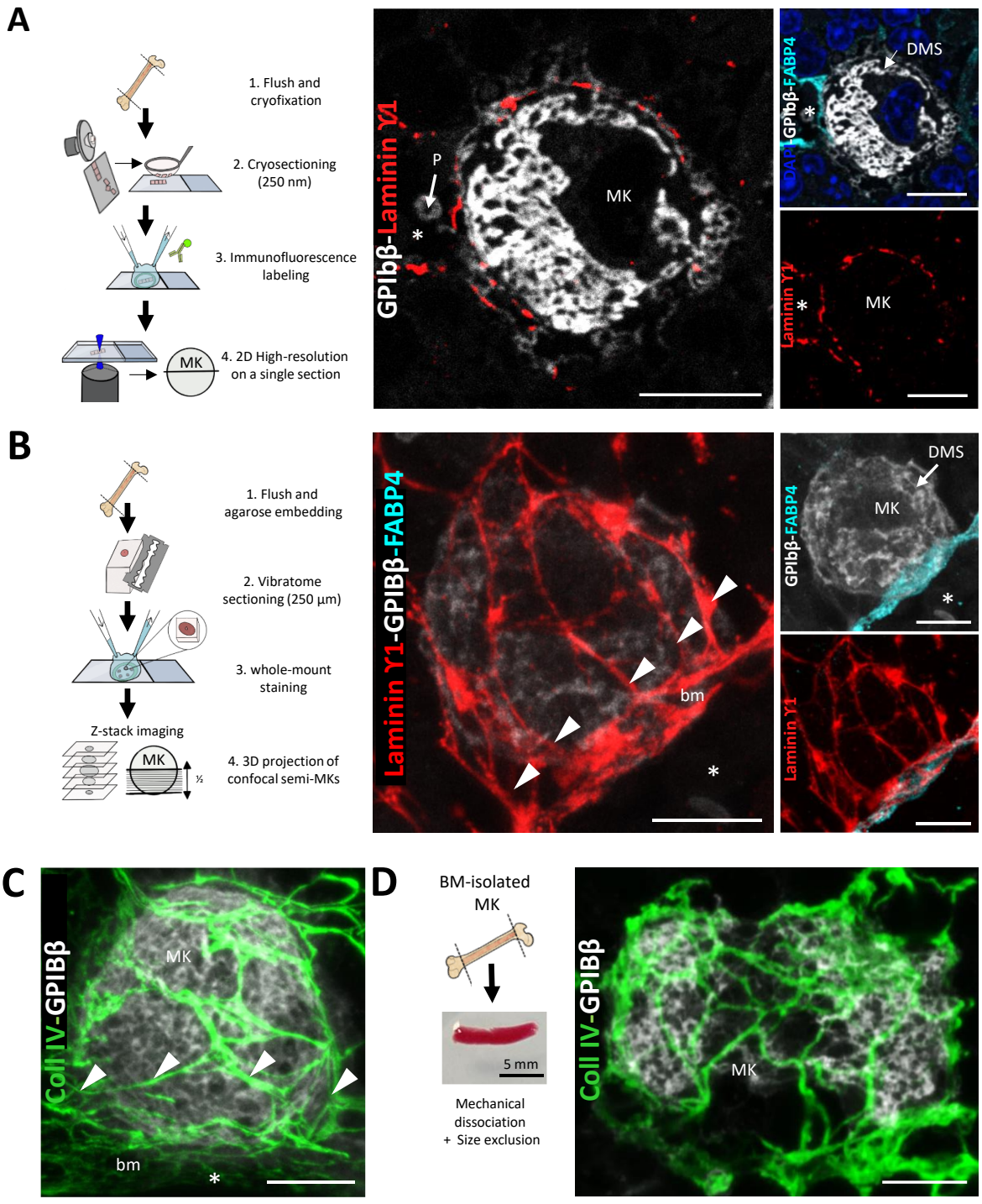
A
1. Flush and cryofixation
2. Cryosectioning (250 nm)
3. Immunofluorescence labeling
MK
4. 2D High-resolution on a single section
GPIbβ-Laminin γ1
P
MK
DAPI-GPIbβ-FABP4
DMS
Laminin γ1
B
1. Flush and agarose embedding
2. Vibratome sectioning (250 µm)
3. whole-mount staining
Z-stack imaging
MK
½
4. 3D projection of confocal semi-MKs
Laminin γ1-GPIBβ-FABP4
bm
GPIbβ-FABP4
DMS
MK
Laminin γ1
C
Coll IV-GPIBβ
MK
bm
D
BM-isolated MK
5 mm
Mechanical dissociation
+ Size exclusion
Coll IV-GPIBβ
MK

Figure 1

LaminiΥ1 and collagen IV form 3D cages of ECM for megakaryocytes, directly connected to the sinusoidal basement membrane

(A) Left panel. Schematic representation of the experimental workflow for 2D imaging of immunostained bone marrow cryosections from WT mice. Confocal imaging is performed on single ultrathin sections with an axial resolution of 250 µm. Right panel. Representative 2D images of a sinusoid-associated megakaryocyte immunostained for laminin Υ1 (red), GPIbβ (white) and FABP4 (cyan). Cell nuclei are visualized with DAPI (blue) (from one out of three independent IF experiments).
(B) Left panel. Schematic representation of the experimental workflow for 3D analysis of whole-mount bone marrow preparations from WT mice. A stack of confocal images covering half the depth of the megakaryocyte is acquired and then z-projected to create a maximum projection image. Right panel. Representative 3D images of sinusoid-associated megakaryocyte immunostained for laminin Υ1 (red), GPIbβ (white) and FABP4 (cyan) (from one out of three independent IF experiments).
(C) Representative 3D images of sinusoid-associated megakaryocyte immunostained for collagen IV (green) and GPIbβ (white).
(D) Bone marrow-isolated megakaryocyte maintaining an ECM cage. Left panel. Schematic of the experimental procedure used to isolate mouse bone marrow megakaryocytes. Right panel. Maximal projection 3D images showing the persistence of the ECM cages (collagen IV in green) around freshly isolated megakaryocytes (GPIbβ in white).

*, sinusoid lumen ; arrowheads, basement membrane-cage connection; BM, bone marrow; bm, basement membrane ; MK, megakaryocyte; Bars, 10 µm**.**

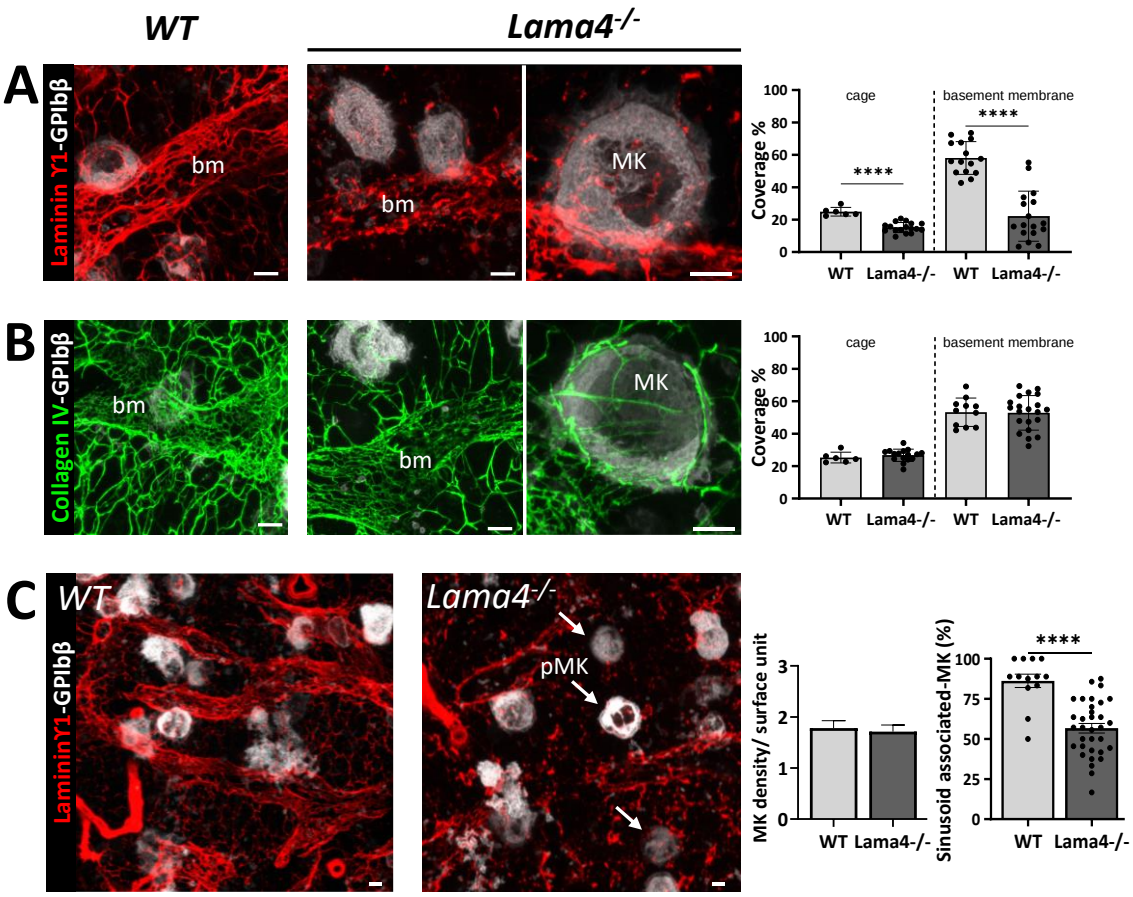

Figure 2

Reduced laminin cage and megakaryocyte-sinusoid interactions in *Lama4*$^{-/-}$ mouse bone marrow.

(A-B) Depletion of laminin α4 leads to a reduction in the laminin ϒ1 deposition, but in collagen IV, in the cage around megakaryocytes and in the sinusoid basement membrane. Left panels. Representative maximal projections showing the immunostaining of laminin γ1 (in red) or collagen IV (in green) in the *Lama4*$^{-/-}$ compared to *WT* mice. Two magnifications are shown for *Lama4*$^{-/-}$ mouse. Right panels. Quantification of laminin γ1 and collagen IV surface coverage per megakaryocyte and per basement membrane surface (laminin: 6<cage<17 and 15<bm<17; collagen IV: 6<cage<16 and 11<bm<21 expressed as a percentage, ****P>0.001 unpaired t-Test).
(C) Depletion of laminin α4 leads to a decrease in the sinusoid-associated megakaryocytes. Left panels. Representative maximal projections showing the immunostaining of laminin γ1 (in red) or megakaryocytes (GPIbβ in white) in the bone marrow of *Lama4*$^{-/-}$ and WT mice. Right panels. Quantification of the total number of megakaryocytes per surface unit (s.u., 12,945 µm^2, n=3 for each genotype) and of sinusoid-associated megakaryocytes (n=3, ****P>0.001 unpaired t-Test) in WT (grey) and *Lama4*$^{-/-}$ (dark) mice. Arrows point to megakaryocytes which are not associated with sinusoids (pMK).

bm, basement membrane; MK, megakaryocyte; pMK, MK in the parenchyma; Bar, 10 µm.

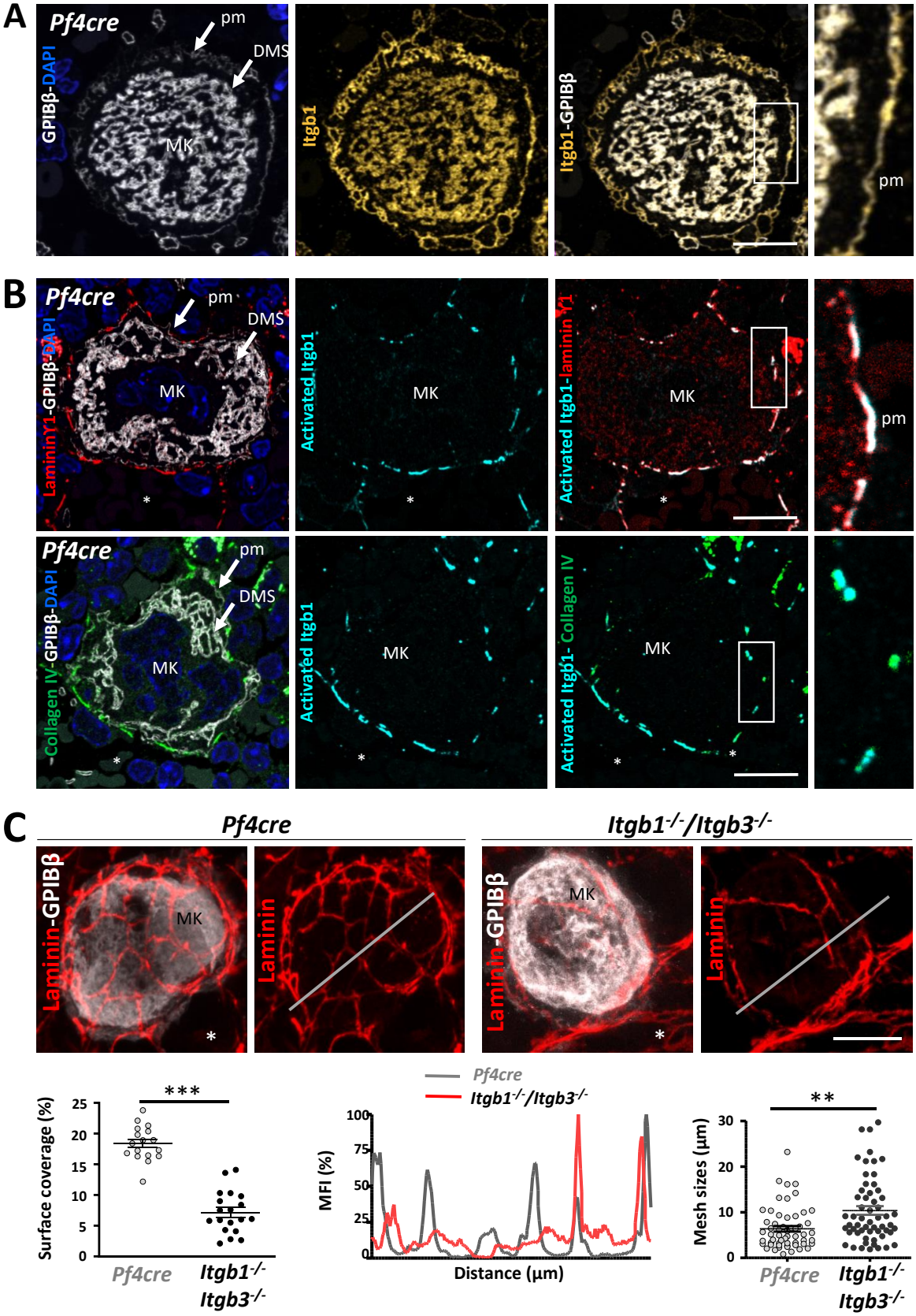
A
Pf4cre
pm
DMS
MK
GPIBβ-DAPI
Itgb1
Itgb1-GPIBβ
pm
B
Pf4cre
pm
DMS
MK
LaminiNγ1-GPIBβ-DAPI
Activated Itgb1
MK
Activated Itgb1-laminin γ1
MK
pm
Pf4cre
pm
DMS
MK
Collagen IV-GPIBβ-DAPI
Activated Itgb1
MK
Activated Itgb1- Collagen IV
MK
C
Pf4cre
Itgb1-/-/Itgb3-/-
Laminin-GPIBβ
MK
Laminin
Laminin-GPIBβ
MK
Laminin
***
Surface coverage (%)
25
20
15
10
5
0
Pf4cre
Itgb1-/-
Itgb3-/-
Pf4cre
Itgb1-/-/Itgb3-/-
MFI (%)
100
75
50
25
0
Distance (µm)
**
Mesh sizes (µm)
30
20
10
0
Pf4cre
Itgb1-/-
Itgb3-/-

Figure 3

Integrin-mediated control of the 3D ECM cage around megakaryocytes

(A) Representative 2D images of *Pf4cre* bone marrow cryosections (250 nm) showing a sinusoid-associated megakaryocyte immunostained for β1 integrin (MAB1997 in yellow). Right: the boxed area is shown at a higher magnification.
(B) Activated β1 integrins form functional adhesion structures around megakaryocyte surfaces. Representative 2D images of *Pf4cre* bone marrow cryosections showing a sinusoid-associated megakaryocyte immunostained for activated β1 integrin (9EG7 in cyan), for GPIbβ (white) and laminin (red, upper panels) or collagen IV (green, lower panels). Right: Magnification of the boxed area showing co-localization of laminin and 9EG7.
(C) Depletion of β1 and β3 integrins leads to a reduction in the laminin deposition on the surface of megakaryocytes. Upper panels. Representative 3D images showing a decrease in laminin deposition (red) on *Itgb1*$^{-/-}$/*Itgb3*$^{-/-}$ megakaryocytes compared to *Pf4cre.* Top panels. (Left) Quantification of laminin surface coverage per megakaryocyte (in %, 17<n<19 as indicated in the bars, ***P>0.001 unpaired t-Test), (Middle) expression profile of the laminin staining along straight-lines (25 µm long) visible as white lines in the confocal images, and (Right) quantification of mesh sizes (in µm, 14<n<16, **P<0.01 Mann-Whitney).

*, sinusoid lumen; MFI, mean fluorescence intensity; MK, megakaryocyte; pm, plasma membrane; Bars, 10 µm.

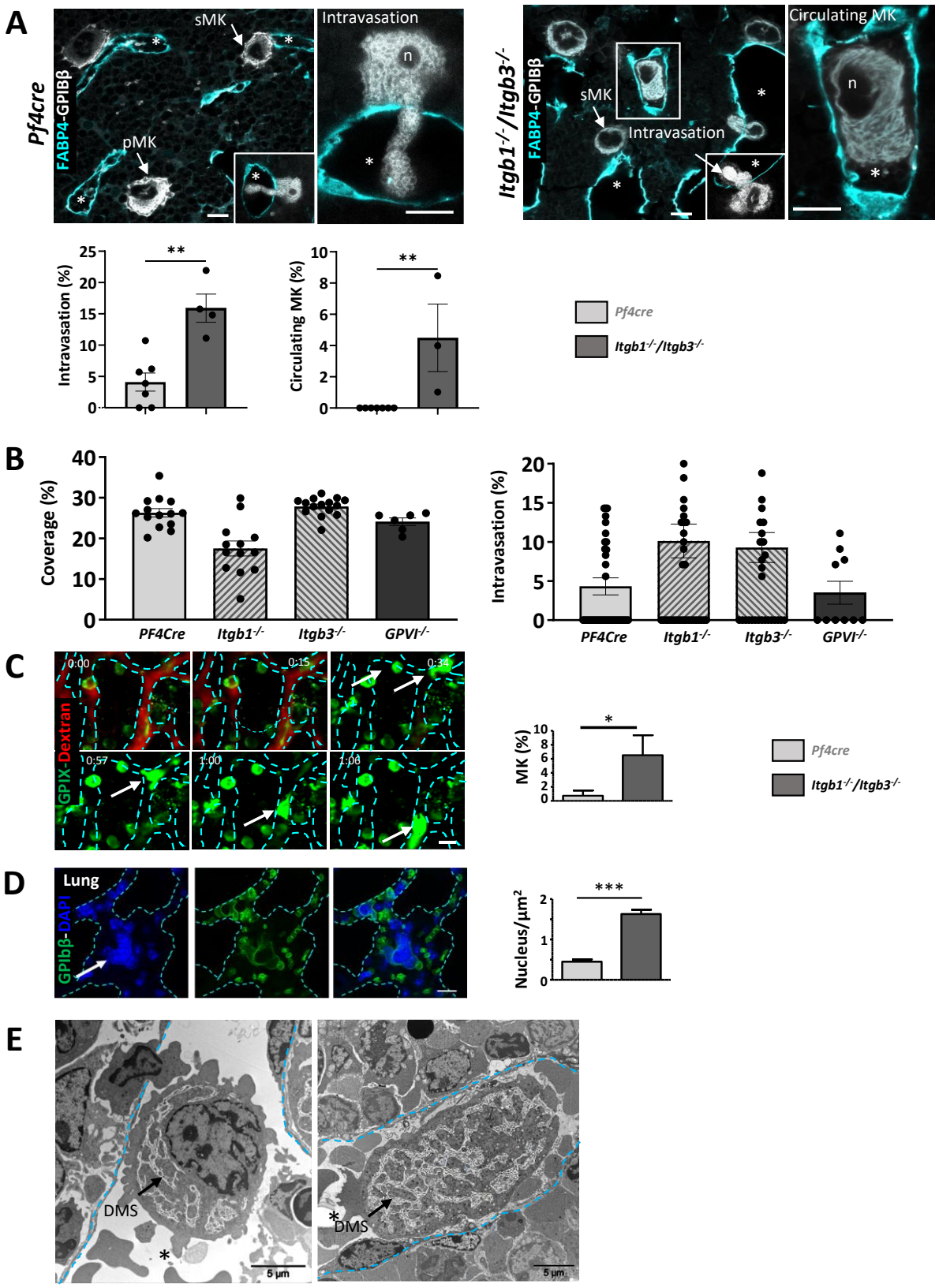
A
Pf4cre
FABP4-GPIBβ
sMK
pMK
Intravasation
n
Itgb1-/-/Itgb3-/-
Circulating MK
Intravasation (%)
Circulating MK (%)
**
Pf4cre
Itgb1-/-/Itgb3-/-
B
Coverage (%)
PF4Cre
Itgb1-/-
Itgb3-/-
GPVI-/-
C
GPIX-Dextran
0:00
0:15
0:34
0:57
1:00
1:08
MK (%)
*
D
Lung
GPIbβ-DAPI
Nucleus/µm2
***
E
DMS
5 µm

Figure 4

Integrins protects megakaryocytes from entering the bloodstream as whole cells

(A) Higher proportion of intravasation events in mice lacking β1/β3 integrins. Upper panel. Representative confocal images of *Pf4cre* and *Itgb1*$^{-/-}$/*Itgb3*$^{-/-}$ whole-mount bone marrow immunostained for GPIbβ (white) and FABP4 (cyan). Top panel. Quantification of megakaryocyte intravasation and circulating megakaryocytes (3 mice minimum for each genotype, 213<n<397 for Pf4cre and *Itgb1*$^{-/-}$/*Itgb3*$^{-/-}$, ** P<0.001 Mann Whitney).
(B) Left panel. Quantification of the laminin γ1 deposition in the ECM cage in single knockout integrins and in GPVI knockout. Right panel. Quantification of the intravasation events in single knock-out mice showing that both integrins are essential for the proper anchoring of megakaryocytes in their vascular niche.
(C) Intravital two-photon imaging of *Itgb1*$^{-/-}$/*Itgb3*$^{-/-}$ mouse calvarial bone marrow stained with intravenously injected AF488-conjugated anti-GPIX antibody and rhodamin dextran. The white arrow indicates an intrasinusoidal *Itgb1*$^{-/-}$/*Itgb3*$^{-/-}$ megakaryocyte, dotted lines illustrate the sinusoid wall and the values in the left corner show the time-lapses. Quantification of circulating megakaryocytes, expressed as a percentage of the total number of megakaryocyte (from 3 independent experiments, 130<n<136 as indicated in the legend, P<0.05, Mann-Whitney).
(D) Increased number of pyrenocytes (arrow, GPIbβ green, DAPI nucleus) within the pulmonary microvessels of *Itgb1*$^{-/-}$/*Itgb3*$^{-/-}$ mice. Cyan dotted lines indicate the vessel wall. Quantification of the intravascular pyrenocytes (from 5 independent experiments, 28<n<149 as indicated in bars, ***P*<0.01, Mann-Whitney).
(E) Two TEM image showing intravascular entire *Itgb1*$^{-/-}$/*Itgb3*$^{-/-}$ megakaryocyte.

*, sinusoid wall; FG, fibrinogen; FN, fibronectin; FG, fibrinogen; n, nucleus; sMK, sinusoid-associated MK; pMK, MK in the parenchyma; PPT, proplatelets; Bars in A-G, 10 µm; Bar in E, 5 µm; Bar in G, 30µm.

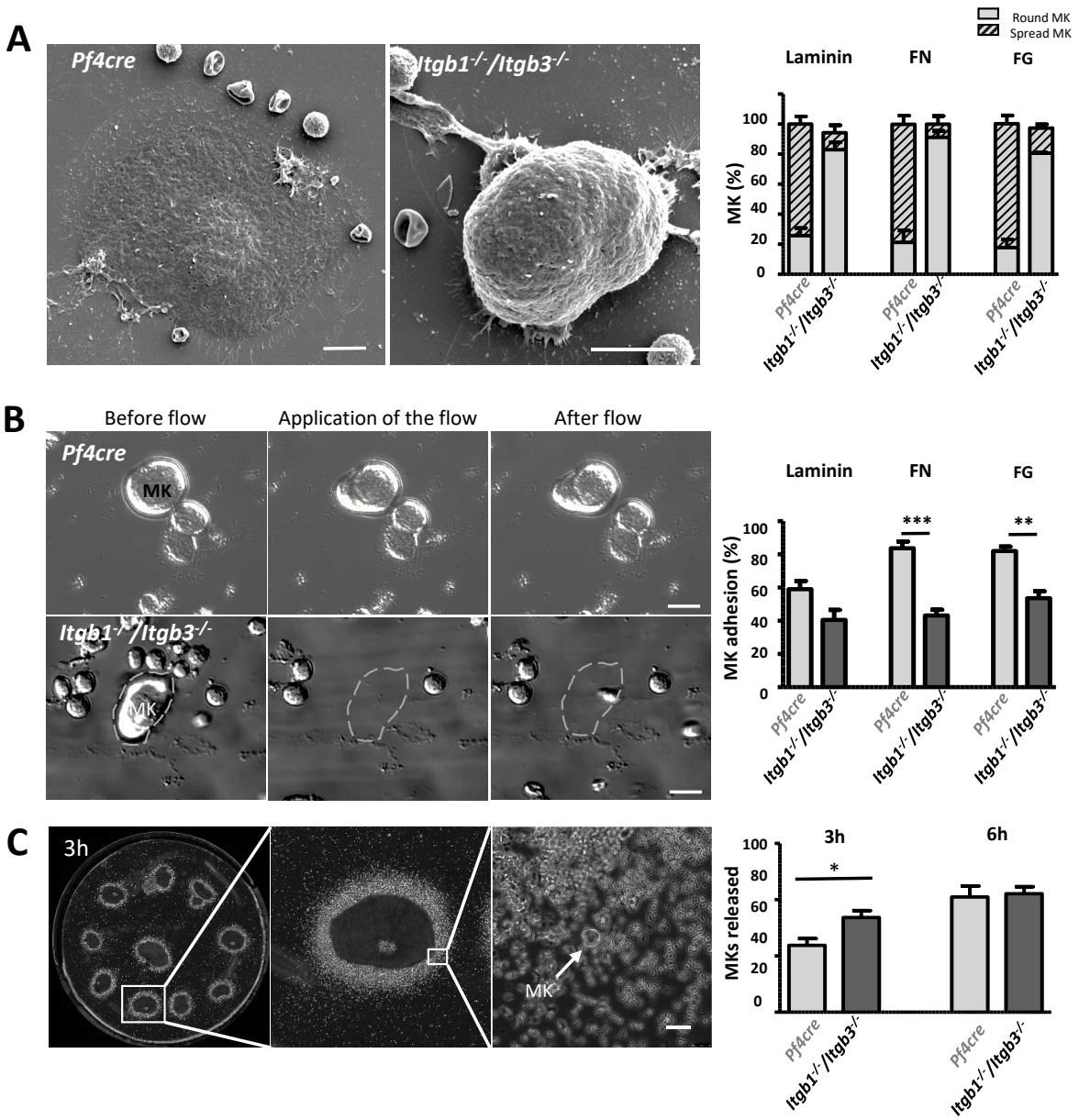
A
Pf4cre
Itgb1-/-/Itgb3-/-
Round MK
Spread MK
Laminin
FN
FG
MK (%)
100
80
60
40
20
0
Pf4cre
Itgb1-/-/Itgb3-/-
B
Before flow
Application of the flow
After flow
MK
MK adhesion (%)
***
**
C
3h
6h
MKs released
*

Figure 5

Integrins promote megakaryocyte adhesion to the ECM components of the bone marrow

(A) Impaired adhesion and spreading of *Itgb1*$^{-/-}$/*Itgb3*$^{-/-}$ MK. Representative SEM images depicting bone marrow-derived megakaryocytes adhering on laminin. Spreading (hatched bars) and round (grey bars) megakaryocytes were counted following 3h incubation on laminin, fibronectin (FN), and fibrinogen (FG) (in %) (from 4-6 independent experiments).
(B) Microfluidic flow chamber to study megakaryocyte adhesion efficiency. Representatives bright field images showing that upon flow application, *Itgb1*$^{-/-}$/*Itgb3*$^{-/-}$ megakaryocytes detach from fibrillary fibronectin protein, while *Pf4Cre* MKs remain attached. Quantification of the detachment of *Pf4cre* and *Itgb1*$^{-/-}$/*Itgb3*$^{-/-}$ megakaryocytes on laminin, fibrillar fibronectin and fibrinogen (from 5 to 7 independent experiments ,**P<0.01, ***P<0,001, Mann-Whitney).
(C) Reduced physical anchoring of *Itgb1*$^{-/-}$/*Itgb3*$^{-/-}$ megakaryocytes to BM. Representatives bright field images of the ten femur BM sections placed in an incubation chamber (left panel), of the box (center panel) and of the megakaryocytes released from the periphery of the explants (right panel). Quantification of the number of *Pf4cre* and *Itgb1*$^{-/-}$/*Itgb3*$^{-/-}$ megakaryocytes released from the explants following 3h (from 10 to 13 independent experiments, 594<n<1095 for Pf4cre and *Itgb1*$^{-/-}$/*Itgb3*$^{-/-}$, *P<0.05, unpaired t-test).

dotted lines, MK detachment; MK, megakaryocytes, FN, fibronectin; FG, fibrinogen; MK, megakaryocytes, n, number of cells studied; Bars in A, 10 µm; Bars in B, 20 µm; Bars in B, 30 µm.

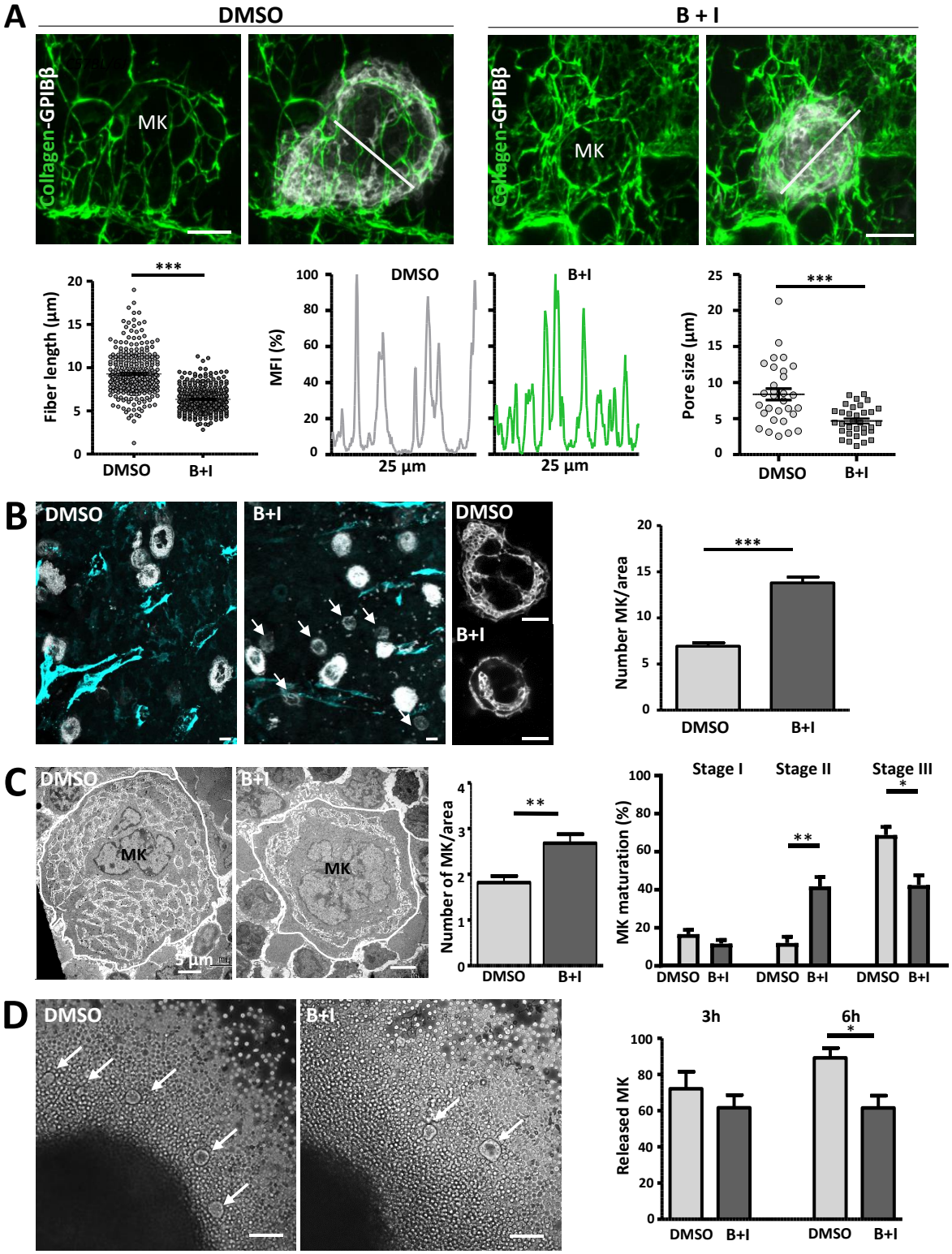
A
DMSO
B + I
Collagen-GPIBβ
MK
Fiber length (µm)
***
DMSO
B+I
MFI (%)
25 µm
Pore size (µm)
B
Number MK/area
C
Number of MK/area
**
MK maturation (%)
Stage I
Stage II
Stage III
*
D
Released MK
3h
6h

Figure 6

Maturation of the 3D ECM cage is correlated with maturation of the DMS in megakaryocytes

(A) MMP inhibition leads to a densification of the 3D ECM cage. Upper panels. Representative 3D confocal images showing a significant increase in collagen IV deposition (green) on the megakaryocyte surface in treated mice treated with the intravenous cocktail of protease inhibitors (B + I). Top panels. (Left) Quantification of collagen IV fluorescence showed a shortening of collagen IV fibers in treated mice compared to that in control mice (from 3-5 independent experiments, 20<n<22 as indicated in the bars, ***P<0;001, Mann-Whitney), (Middle) Histograms of fluorescence intensity versus distance showed an increase in cross-linking with a reduction in pore size (white lines of 25µm length are visible in the confocal images), (Right) Reduction in mesh sizes in treated mice (from 3 independent experiments, 7<n<12, ***P>0.001, t-test).
(B) MMP inhibition affects megakaryocyte growth (indicated by arrows). Representative confocal images from DMSO *vs* B+I treated mice immunostained for GPIbβ (white) and FABP4 (cyan), zoomed-in images showing the difference in megakaryocyte size between the two groups. Quantification of the number of megakaryocytes per bone marrow area (194 x 194 µm) (from 3 independent experiments, 229<n<483 as indicated in the bars, ***P<0.0001, Mann-Whitney).
(C) TEM observation revealed the presence of numerous immature megakaryocytes (stage II) in treated mice as compared to fully mature megakaryocytes in control mice (stage III). (Middle) Quantification of the total number of megakaryocyte s (145<n<169 as indicated in bars, **P<0.01, Mann-Whitney) and in the proportion of immature megakaryocytes (stage II) in the B + I group (from 3 independent experiments, *P < 0.05, **P < 0.01, one way ANOVA Dunn's).
(D) Representatives bright field images of the megakaryocytes (arrows) released from the periphery of the control and treated explants. Quantification of the number of megakaryocytes released following 3h and 6h (from 6 independent experiments, 370<n<783 for DMSO and B+I, *P<0.05, unpaired t-test).

B + I, batimastat + Ilomastat; sMK, sinusoid-associated MK; pMK, MK in the parenchyma; n, number of cells studied; Bars in A and B, 10 µm; Bars in C, 5 µm; Bar in D, 50 µm.

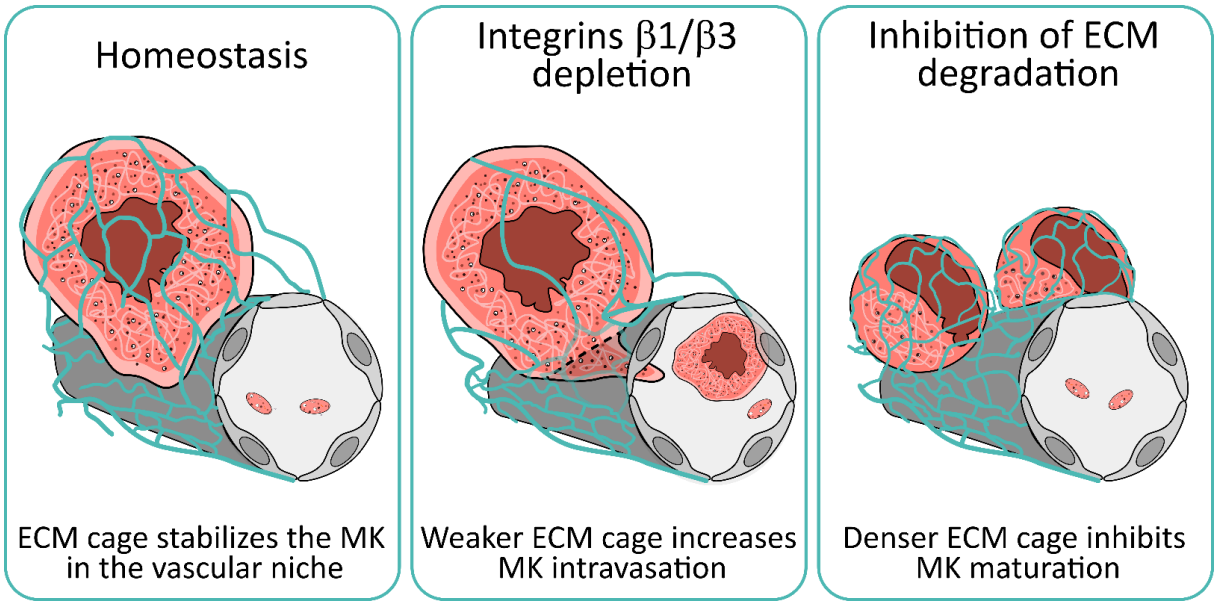

Figure 7

Integrin-mediated signaling and MMP proteolysis regulate the matrix remodeling and the adhesive properties of the 3D ECM cage, which control megakaryocyte maturation and intravasation at the bone marrow-blood interface.